ChemPhysChem

Research Article
doi.org/10.1002/cphc.202400495

Chemistry Europe
European Chemical Societies Publishing

www.chemphyschem.org

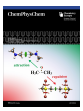

Attraction versus Repulsion between Methyl and Related Groups: $(CH_3NHCH_3)_2$ and $(CH_3SeBr_2CH_3)_2$

Mariusz Michalczyk,*[a] Steve Scheiner,[b] and Wiktor Zierkiewicz[a]

The starting point for this work was a set of crystal structures containing the motif of interaction between methyl groups in homodimers. Two structures were selected for which QTAIM, NCI and NBO analyses suggested an attractive interaction. However, the calculated interaction energy was negative for only one of these systems. The ability of methyl groups to interact with one another is then examined by DFT calculations. A series of $(CH_3PnHCH_3)_2$ homodimers were allowed to interact with each other for a range of Pn atoms N, P, As, and Sb. Interaction energies of these C···C tetrel-bonded species were below 1 kcal/mol, but could be raised to nearly 3 kcal/mol if the C atom was changed to a heavier tetrel. A strengthening of the C···C intermethyl bonds can also be achieved by introducing an asymmetry via an electron-withdrawing substituent on one unit and a donor on the other. The attractions between the methyl and related groups occur in spite of a coulombic repulsion between σ-holes on the two groups. NBO, AIM, and NCI tools must be interpreted with caution as they can falsely suggest bonding when the potentials are repulsive.

Introduction

In recent decades, there have been significant advancements in our understanding of noncovalent interactions. This progress can be attributed to the rapid development in computational chemistry methods and the collaboration between experimental and theoretical approaches in predicting crystal-derived structures. In addition to the well-known hydrogen bonding,[1] new noncovalent interactions have started to be identified in crystal structures and theoretical models. The introduction of σ-hole and π-hole concepts[2] brought a significant increase in the literature reports on Lewis acid-Lewis base pairwise interactions which were named according to the family of the periodic table that contains the hole donor.[3] Among the newly recognized contacts is the tetrel bond (TB), in which an atom from group 14 participates in interactions with electron-rich units. Recently, numerous studies have explored the characteristics of tetrel bonding,[4] as well as the possible uses of systems stabilized by tetrel bonds. Among them the participation in protein-drug or anion recognition,[5] assembling and maintaining the supramolecular architectures,[6] crystal engineering[7] or explaining the mechanism of S_N2 organic reaction[8] can be mentioned.

An extremely interesting variant of the tetrel bond is the ditetrel bond which was discovered recently and described in a few papers.[9] The occurrence of an interaction between atoms of the same group (or even among identical atoms as in the case of methyl···methyl interactions) prompts examination of the influence of substituents attached to tetrel atoms as the underlying reason for this contact. It is well known that electron-withdrawing neighbors induce the growth of the σ-hole/π-hole magnitude and consequently increase of the electrophilicity of the Lewis acid while the electron-donating groups cause the opposite effect. Therefore, ditetrel bonds were observed for tetrels of metallic nature as Sb or Sn[9a] when appropriately selected substituents were bound to the tetrel atoms at both ends of the complex subunits. As a root of such interaction the donation of electron density from T lone pair or T–R bonding orbital to the σ-hole region has been identified.[9a]

The aforementioned interactions between methyl groups are an especially intriguing case that merits further investigation. First of all, chemistry relies heavily on the presence of methyl groups, which serve as functional groups in organic synthesis. Methyl groups can be found in various naturally occurring substances like DNA and hormones.[10] These moieties contribute to the structure and reactivity of molecules, e.g. enhanced stability of DNA is commonly linked to hydrophobic interactions between water molecules and the methyl group.[11] They also play a role in establishing the physical properties of molecules, such as solubility and boiling point. Secondly, theoretical studies on interactions between methyl groups are scarce in the literature.[12] In general, sp^3 carbon atoms are mostly categorized as Lewis acids in tetrel bonding when the nucleophile is approaching the carbon-containing molecule,[4b,c,6b,13] less frequently as electron donors (Lewis bases),[14] for example in the E-CH_3···H–Y hydrogen bonds where E=B, Al, Ga, In, Tl, Si, Ge, Sn, Pb and Y=N, O, S, Se[15] or in alkali metals···methyl interactions found in aluminates.[16]

The well-defined function of methyl groups as either electron acceptors or donors,[17] depending on their chemical surroundings, significantly restricts the conditions for methyl···methyl interactions. In 2014, Zhou *et al.* asked a question regarding the interaction between methyl groups.[12a] In the set of XCH_3···CH_3BH_2 (X=F, CN, NO_2, HCO, and $SOCH_3$) complexes

[a] M. Michalczyk, W. Zierkiewicz
Faculty of Chemistry, Wrocław University of Science and Technology,
Wybrzeże Wyspiańskiego 27, 50-370 Wrocław, Poland
E-mail: mariusz.michalczyk@pwr.edu.pl

[b] S. Scheiner
Department of Chemistry and Biochemistry, Utah State University Logan,
Utah 84322-0300, United States

Supporting information for this article is available on the WWW under https://doi.org/10.1002/cphc.202400495

weak noncovalent interactions between $-CH_3$ groups in range from −3 to −2 kcal/mol were detected and classified as van der Waals interactions due to the pivotal role of dispersion forces. It is worth mentioning that when the carbon atom in the methyl moiety was switched to a heavier tetrel the absolute values of interaction energy rose to 4.5–5.5 kcal/mol. Attractive dimethyl interactions were very recently examined by Keshtkar *et al.*[12b] based on the Cambridge Structure Database (CSD) survey. Statistical analysis of CSD outcomes revealed common trends in the geometry of methyl···methyl stabilized dimers in terms of C···C distances and bonding angles; the most frequent distances were around 3.5 Å and angles were placed in the 150–180° span. The theoretical predictions for 12 selected heteroadducts with structural motif of E-CH_3···CH_3-Y (E=Al, Si, Sn; Y=CH_3, $N(CH_3)_2$, OCH_3, Br) are characterized by very small interaction energies ranging between −1.2 and −0.5 kcal/mol, the strongest for E=Al and Y=Br. The attractive character of each interaction was supported by the presence of C···C bond paths in the QTAIM analysis and interaction between orbitals in pattern: σ(E–C)→σ*(C–Y) found by the NBO approach. The authors postulated that model complexes are stabilized by electrostatics with involvement of charge transfer and polarization.

In the current work, we decided to go a step further than our predecessors. It is obvious that a weak interaction between methyl groups happens when they are combined with different substituents of opposite nature. We questioned whether it is possible that such an interaction occurs in homodimers. An attraction between identical monomers seems problematic as their equivalency induces a strong obstacle to creating attractive electrostatic forces or electron transfer. We wondered then as to why the CSD contained close methyl···methyl contacts. We set about to analyze them by means of electron density topology methods such as QTAIM and NCI, as well as the NBO protocol. Model complexes based on the X-ray framework were further processed via quantum chemical methods to assess the strength and nature of interactions between methyl groups and related ones in the group of homodimers in which the carbon atom was substituted by heavier tetrels. Other systems probed were heterodimers with asymmetric placement of substituents. One pressing question concerns whether the QTAIM, NCI and NBO analyses should perhaps be interpreted with caution as they can misleadingly label repulsive interactions as attractive, an issue that has arisen recently for other interactions in the literature.[18]

Computational Methods

Quantum calculations were carried out with the M06-2X DFT functional, with the aid of the def2tzvpp[19] basis set within the context of the Gaussian 16 (Rev. C.01) package.[20] The Cambridge crystal structure database (CSD)[21] was used to search experimentally derived geometries with methyl···methyl structural motifs which were further analyzed via quantum chemical methods without any pre-optimization. Harmonic frequency analysis of normal modes verified that the optimized geometries of additional model complexes represent true minima. The counterpoise approach proposed by Boys and Bernardi reduced basis set superposition error (BSSE).[22] The MEP (molecular electrostatic potential) of the isolated monomers was analyzed via MultiWFN software[23] in order to quantify maxima on the 0.001 au isodensity surface. Graphical post-processing of the MEP was performed using VMD software.[24] The MultiWFN program was also employed for the NCI analysis. Using the AIMAll program,[25] the QTAIM analysis of the electron density topology[26] elucidated bond paths and their associated bond critical points. NBO was used to analyze[27] interorbital interactions within complexes. Decomposition of the interaction energy into its components was achieved using the ALMO-EDA protocol.[28]

Results

Methyl···Methyl Interactions

Figure 1 presents the RDG diagrams of these two example systems, with their geometries taken directly from their crystal structures. There is a green region directly between the two methyl C atoms of both systems, indicative of an attractive interaction. This C···C noncovalent bonding scenario is confirmed by QTAIM analysis of the electron density topology which draws a bond path between the two C atoms, with a density ρ_{BCP} at its critical point of 0.004 au, a value typical of such bonding. In addition, the results of the NBO analysis also

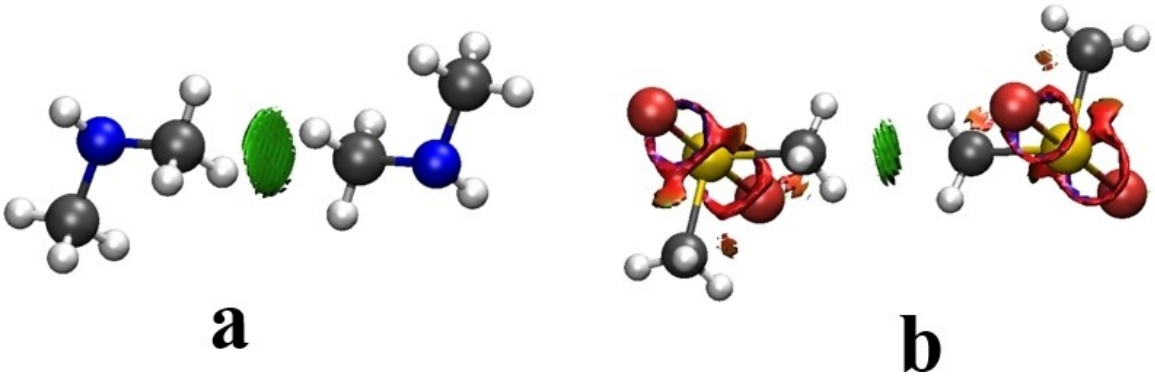

Figure 1. RDG diagrams of a) $(CH_3NHCH_3)_2$ Refcode: NAWYES02[29] and b) $(CH_3SeBr_2CH_3)_2$ Refcode: RIZMIW.[30] R(CC) distances are 3.301 and 3.390 Å in a and b, respectively.

indicate an attractive interaction. In the case of the $(CH_3NHCH_3)_2$ and $(CH_3SeBr_2CH_3)_2$ complexes, the NBO second-order perturbation energies $E^{(2)}$ between the σ(C–H) and σ*(N–C) or σ*(Se–C) orbitals are 0.44 and 0.28 kcal/mol, respectively. The interaction energies of the two systems were computed at four different levels of theory and are presented in Table 1. All results, including the most accurate CCSD(T) support the idea of an attractive force between the two methyl groups of $(CH_3NHCH_3)_2$ but the situation is different for $(CH_3SeBr_2CH_3)_2$ where the positive interaction energy is indicative of a repulsion, despite the QTAIM and RDG suggestions to the contrary.

So as to probe this issue further, the way in which the interaction behaves over a full range of the intermolecular distance was elucidated. An assortment of different measures of the intermolecular interaction was computed for a full range of the C···C distance, holding the remainder of the geometry in its crystal structure. Table 2 lists the relevant information where R(C···C) varies from 1 Å shorter than its X-ray distance up to 1 Å longer.

The interaction energy quickly shifts from attractive at 3.301 Å to repulsive for shorter distances, as much as +22.6 kcal/mol at 2.301 Å. Despite this switchover to repulsion, the various QTAIM markers continue to progressively climb, with the absolute values of ρ, $\nabla^2\rho$, and V reaching up to very large values. The same behavior is observed for the RDG marker of sign(λ_2)ρ as well as the NBO second-order perturbation energy $E^{(2)}$ which measures the charge transfer from the CH bonding orbitals of one unit to the σ*(N–C) of its partner (these values could be doubled since there is charge transfer in both directions). This behavior is shown graphically in Figure 2 so as to better view the rapid rise of these parameters with diminishing R(C···C). A similar pattern arises in the RDG diagrams of Figure 3 wherein the originally shredded light green lobe between the two C atoms for R = 4.301 Å unites and enlarges for the X-ray distance of 3.301 Å, and then acquires a blue color at 2.301 Å, signifying a strong attractive force.

In conclusion the simple evaluation of AIM, NBO, and NCI data would lead to the erroneous conclusion that the compression of the two units closer than their separation in the crystal makes the interaction progressively more attractive, in contrast to a steadily rising repulsion energy. This finding is consistent with recent calculations of a wide variety of other systems involving a H-bond, a halogen bond, a tetrel bond, one involving a Mg···N interaction, and that between the two H atoms of CH_4 dimers.[18b]

Table 1. Interaction energies (kcal/mol, corrected for BSSE) at different levels of theory in the context of the def2TZVPP basis set.

Refcode	M062X	PBE0-D3	MP2	CCSD(T)
$(CH_3NHCH_3)_2$	−0.40	−0.93	−0.34	−0.42
$(CH_3SeBr_2CH_3)_2$	+1.40	+0.17	+0.64	+0.73

Generalized Systems

Given the very weak interactions between methyl groups within the context of NC···CN arrangements, it was considered worthwhile to investigate how these interactions might change if both the N and C atoms were replaced by other pnicogen or tetrel atoms, respectively. Scheme 1 illustrates the general configuration and range of systems considered, covering 16 homodimers in all.

The molecular electrostatic potential (MEP) surrounding these molecules all contain a negative region corresponding to the Pn lone pair, as evident in Figure 4. There is also a less intense red positive σ-hole along the extension of the Pn–T bond. The maximum of the potential on the 0.001 au isodensity surface is denoted V_{max}, and is reported in Table 3. This quantity is largest for Pn≡N, followed by Sb. In most cases, V_{max} is largest for T=Sn.

Full geometry optimizations led to configurations wherein the TH_3 units face each other directly but there is a distinction between the methyl and other TH_3 groups. As shown in Figure 5 for the CH_3AsHCH_3 homodimer, the As–C···C arrange-

Table 2. Selected energetic, QTAIM, NBO and NCI parameters for $(CH_3NHCH_3)_2$ for different distances between subsystems.

R(C···C) (Å)	E_{int} (kcal/mol)	ρ (au)	$\nabla^2\rho$ (au)	V (au)	sign(λ_2)ρ (au)	$E^{(2)}$ (kcal/mol)
2.301	22.59[b]	0.0322	0.1797	−0.0398	−0.0322	10.66[c]
2.501	9.25	0.0218	0.1190	−0.0233	−0.0218	5.44
2.701	3.10	0.0149	0.0772	−0.0139	−0.0149	2.86
2.901	0.60	0.0102	0.0498	−0.0083	−0.0102	1.54
3.101	−0.22	0.0069	0.0323	−0.0050	−0.0069	0.84
3.301[a]	**−0.40**	**0.0045**	**0.0213**	**−0.0030**	**−0.0045**	**0.44**
3.501	−0.41	0.0029	0.0142	−0.0017	−0.0029	-[d]
3.701	−0.38	0.0018	0.0094	−0.0010	−0.0018	-
3.901	−0.34	0.0012	0.0061	−0.0006	−0.0012	-
4.101	−0.30	0.0008	0.0039	−0.0004	−0.0008	-
4.301	−0.25	0.0005	0.0025	−0.0002	−0.0005	-

[a] in geometry of crystal. [b] corrected for BSSE. [c] Σσ(C–H)-σ*(N–C) sum shares from one subunit to another (in both directions). [d] None above threshold 0.05 kcal/mol.

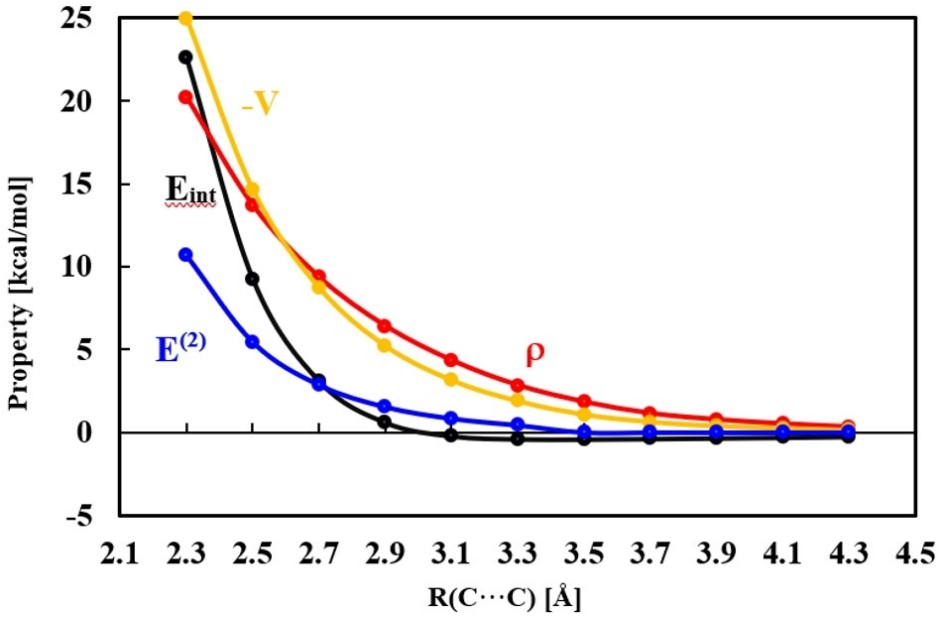

Figure 2. Dependence of various properties of $(CH_3NHCH_3)_2$ on R(C···C) (all quantities in kcal/mol).

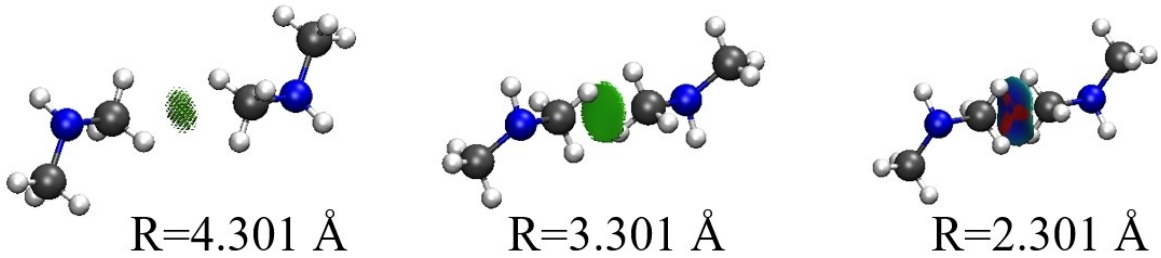

Figure 3. RDG diagrams for $(CH_3NHCH_3)_2$ at indicated R(C··C) distances. Color coding: dark blue–strong noncovalent interactions, green–weak noncovalent interactions, red–steric repulsions. Analyses were made using RDG surface of 0.50 au.

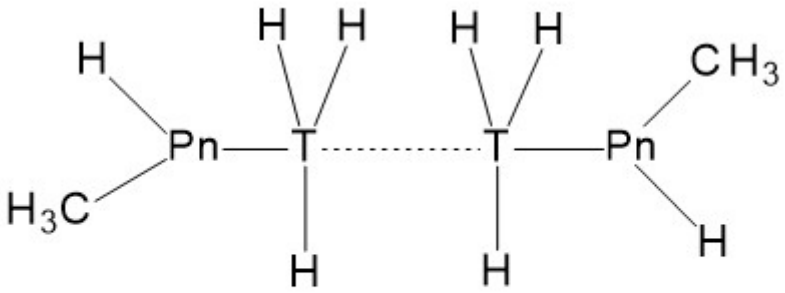

T= C, Si, Ge, Sn
Pn= N, P, As, Sb

Scheme 1. Homodimers examined.

ment is very nearly linear, but the analogous angle is reduced to 160° when the interacting methyls are replaced by GeH_3 in Figure 5b. As may be seen in Table 4 this pattern is characteristic of all of the homodimers. More importantly, the interaction

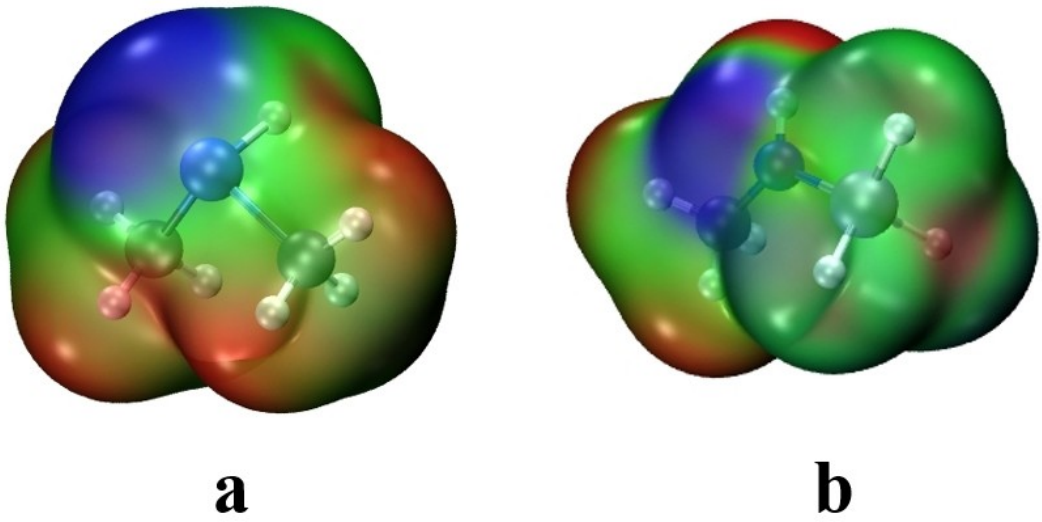

Figure 4. MEP on the 0.001 au isodensity surface for a) CH_3AsHCH_3 and b) CH_3NHSiH_3 Blue and red colors correspond respectively to −12.5 and +12.5 kcal/mol.

Table 3. MEP maximum (V_{max},kcal/mol) at tetrel atom on the 0.001 au isodensity surface for isolated monomers.

Monomer	V_{max} (T)
CH_3NHCH_3	24.7
CH_3NHSiH_3	30.9
CH_3NHGeH_3	27.6
CH_3NHSnH_3	29.6
CH_3PHCH_3	13.0
CH_3PHSiH_3	15.1
CH_3PHGeH_3	15.1
CH_3PHSnH_3	22.3
CH_3AsHCH_3	12.9
$CH_3AsHSiH_3$	14.8
$CH_3AsHGeH_3$	14.8
$CH_3AsHSnH_3$	21.5
CH_3SbHCH_3	19.2
$CH_3SbHSiH_3$	18.6
$CH_3SbHGeH_3$	18.4
$CH_3SbHSnH_3$	19.6

energies in the last column of Table 4 show a weak interaction, less than 1 kcal/mol for methyl groups, but somewhat larger up to 2.8 kcal/mol for bigger T atoms. These quantities are largest for Pn═N, diminishing slowly as Pn grows larger.

The latter deviation from linearity within the Pn─T···T─Pn alignment has a particular effect on the QTAIM bonding paths. As exhibited in Figure 5c, this path directly connects the two C atoms of the methyl groups. The path within the nonlinear system in Figure 5d, on the other hand, connects H atoms on the two TH_3 groups. This pattern is not restricted to the particular homodimers in Figure 5, but is a general feature of all of the systems examined here, as is evident in Figure S1. In other words, QTAIM suggests a ditetrel C···C bond between methyl groups, but finds the other TH_3 groups are bound by attractive H···H interactions. The values of the various QTAIM parameters supplied in Table 5 are not easily reconcilable with the stronger interactions between TH_3 groups other than methyl revealed by E_{int}. In all cases, the positive values of both $\nabla^2\rho$ and H are consistent with a fully noncovalent bond.

Another viewpoint concerning noncovalent interactions arises in the NBO context of interorbital interactions. The source of transfers across from one molecule to the other are the σ(TH) orbitals, which wind up in the σ*(T─Pn) antibonding orbital. These quantities displayed in the last column of Table 5 find a sizable degree of transfer for the atoms larger than C, but much less for the latter. $E^{(2)}$ is largest for Pn═N, but there is not much sensitivity to the identity of the T atom. In contrast to the QTAIM bond paths which directly connect C atoms, with H···H connections for the heavier T, NBO suggests an opposite interpretation of T···T bonds only for the larger T atoms.

Decomposition of the total interaction energy into its major components offers an alternative perspective. The results of such a decomposition by the ALMO-EDA scheme presented in Table 6 depend to a large extent on the nature of the pnicogen atom. In the case of the Pn═N systems in the upper section of the table, the electrostatic and dispersion terms provide comparable contributions. The systems containing P, As, and Sb differ in that they depend more heavily on dispersion. This latter distinction is most marked in the intermethyl interactions where dispersion contributes some 70% to the sum of attractive components, down to roughly half for the other T atoms. The charge transfer represents a smaller component, particularly for methyl interactions, a trend which is consistent with the NBO data. Polarization contributions are particularly small, in the neighborhood of 5%.

With specific regard to the electrostatic term, this quantity is negative in all cases, despite the near superposition of the σ-holes on the TH_3 groups. There are several reasons for this. In the first place the two interacting TH_3 groups do not perfectly

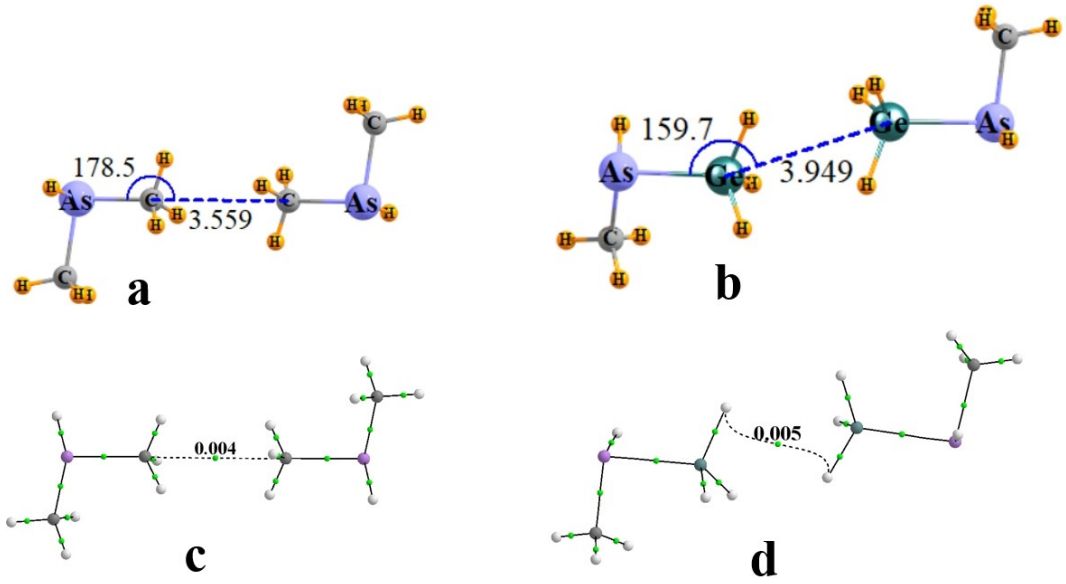

Figure 5. Optimized geometries of a) $(CH_3AsHCH_3)_2$ and b) $(CH_3AsHGeH_3)_2$. Distances in Å, angles in degs; c and d show QTAIM molecular diagrams of the same systems, with ρ_{BCP} in au.

Table 4. Intermolecular distances (Å), and angles (degs), and interaction energies (kcal/mol) of homodimers.

Homodimer	R(T···T)	θ(Pn–T···T)	E_{int}
$(CH_3NHCH_3)_2$	3.392	177.3	−0.60
$(CH_3NHSiH_3)_2$	3.673	158.2	−2.20
$(CH_3NHGeH_3)_2$	3.801	156.4	−2.04
$(CH_3NHSnH_3)_2$	4.000	154.5	−2.78
$(CH_3PHCH_3)_2$	3.534	174.2	−0.42
$(CH_3PHSiH_3)_2$	3.814	158.8	−1.41
$(CH_3PHGeH_3)_2$	3.940	156.5	−1.45
$(CH_3PHSnH_3)_2$	4.128	153.8	−2.05
$(CH_3AsHCH_3)_2$	3.559	177.4	−0.41
$(CH_3AsHSiH_3)_2$	3.823	158.7	−1.36
$(CH_3AsHGeH_3)_2$	3.949	159.7	−1.35
$(CH_3AsHSnH_3)_2$	4.136	153.8	−2.01
$(CH_3SbHCH_3)_2$	3.607	179.2	−0.39
$(CH_3SbHSiH_3)_2$	3.859	159.3	−1.25
$(CH_3SbHGeH_3)_2$	3.984	159.4	−1.35
$(CH_3SbHSnH_3)_2$	4.170	154.2	−1.88

align, with θ(Pn–T···T) angles less than 180° (see Table 4). As another point, the ELEC term is derived from more than just the direct interaction between σ-holes, but represents contact between wider swaths of the two subunits. Finally, charge penetration acts to make this term more negative than if it were absent.

The displacement of electron density that accompanies the interaction can be visualized by a density difference map that subtracts the density of the two separate monomers from that of the full complex. These difference maps in Figure 6 indicate density gains and losses by red and blue colors, respectively. The contour shown in all cases is the same 0.0001 au so as to enable comparisons from one system to the other. The interactions between the methyl groups in Figure 6a are clearly smaller in magnitude than those for the larger T atoms, which are fairly consistent amongst themselves. But the patterns in all cases are qualitatively similar. There is a red buildup of density between the two T atoms, consistent with the formation of a bonding interaction. This density accrual is compensated by losses in more peripheral regions.

Table 5. QTAIM selected parameters for C···C interactions (au) and NBO second-order perturbation energies $E^{(2)}$ (sums in both directions of electron flow; kcal/mol).

Homodimer	ρ	$\nabla^2\rho$	V	H	$E^{(2)}$
$(CH_3NHCH_3)_2$	0.008[a]	0.038[a]	−0.0052[a]	0.0022[a]	0.48
$(CH_3NHSiH_3)_2$	0.009[b]	0.024	−0.0047	0.0006	2.65
$(CH_3NHGeH_3)_2$	0.007[b]	0.020	−0.0034	0.0009	3.22
$(CH_3NHSnH_3)_2$	0.008[b]	0.018	−0.0032	0.0007	2.63
$(CH_3PHCH_3)_2$	0.004	0.016	−0.0020	0.0009	0.17
$(CH_3PHSiH_3)_2$	0.007[b]	0.018	−0.0030	0.0007	1.43
$(CH_3PHGeH_3)_2$	0.006[b]	0.015	−0.0022	0.0008	1.63
$(CH_3PHSnH_3)_2$	0.006[b]	0.015	−0.0024	0.0006	1.51
$(CH_3AsHCH_3)_2$	0.004	0.015	−0.0019	0.0009	-
$(CH_3AsHSiH_3)_2$	0.006[b]	0.017	−0.0029	0.0007	1.27
$(CH_3AsHGeH_3)_2$	0.005[b]	0.015	−0.0021	0.0008	1.45
$(CH_3AsHSnH_3)_2$	0.006[b]	0.014	−0.0023	0.0006	1.45
$(CH_3SbHCH_3)_2$	0.004	0.013	−0.0018	0.0008	0.12
$(CH_3SbHSiH_3)_2$	0.006[b]	0.016	−0.0025	0.0007	1.10
$(CH_3SbHGeH_3)_2$	0.005[b]	0.014	−0.0019	0.0007	1.18
$(CH_3SbHSnH_3)_2$	0.006[b]	0.013	−0.0021	0.0006	1.32

[a] sum of parameters for two equivalent C···C bond paths between carbon atoms (see Figure S1). [b] all parameters in this row are given for H···H bond paths, no C···C bond path detected (see Figure S1).

Table 6. ALMO-EDA decomposition of interaction energies (kcal/mol). ELEC = electrostatic term, PAULI=Pauli repulsion, DISP = dispersion, POL = polarization, CT = charge transfer. Percentage contributions are listed as fraction of sum of attractive elements.

Homodimers	E_{int}	ELEC	%	PAULI	DISP	%	POL	%	CT	%	Total
$(CH_3NHCH_3)_2$	−0.60	−1.89	52	3.04	−1.52	42	−0.09	2	−0.14	4	−0.59
$(CH_3NHSiH_3)_2$	−2.20	−2.64	32	6.00	−3.79	46	−0.39	5	−1.36	17	−2.20
$(CH_3NHGeH_3)_2$	−2.04	−3.92	45	6.68	−3.40	39	−0.48	5	−0.92	11	−2.04
$(CH_3NHSnH_3)_2$	−2.78	−3.54	37	6.88	−4.01	41	−0.66	7	−1.46	15	−2.78
$(CH_3PHCH_3)_2$	−0.42	−0.44	24	1.44	−1.26	68	−0.07	4	−0.09	5	−0.42
$(CH_3PHSiH_3)_2$	−1.41	−1.70	30	4.30	−2.88	50	−0.26	5	−0.87	15	−1.41
$(CH_3PHGeH_3)_2$	−1.45	−1.77	32	4.03	−2.84	52	−0.32	6	−0.55	10	−1.45
$(CH_3PHSnH_3)_2$	−2.05	−2.51	33	5.54	−3.59	47	−0.39	5	−1.10	15	−2.05
$(CH_3AsHCH_3)_2$	−0.41	−0.40	23	1.35	−1.22	69	−0.06	3	−0.09	5	−0.41
$(CH_3AsHSiH_3)_2$	−1.36	−1.63	29	4.19	−2.80	51	−0.24	4	−0.88	16	−1.36
$(CH_3AsHGeH_3)_2$	−1.35	−1.57	31	3.76	−2.71	53	−0.31	6	−0.53	10	−1.35
$(CH_3AsHSnH_3)_2$	−2.01	−2.42	33	5.42	−3.53	48	−0.38	5	−1.09	15	−2.00
$(CH_3SbHCH_3)_2$	−0.39	−0.37	21	1.38	−1.26	71	−0.06	3	−0.08	4	−0.39
$(CH_3SbHSiH_3)_2$	−1.25	−1.59	29	4.20	−2.84	52	−0.21	4	−0.81	15	−1.25
$(CH_3SbHGeH_3)_2$	−1.35	−1.58	30	3.83	−2.84	55	−0.26	5	−0.51	10	−1.36
$(CH_3SbHSnH_3)_2$	−1.88	−2.33	32	5.29	−3.48	48	−0.32	4	−1.05	15	−1.88

Heterodimers

Since the σ-holes of the two methyl groups face one another directly, one might expect that the any weakening of these holes might reduce the coulombic repulsion and possibly strengthen the overall interaction. In order to test this supposition, a series of heterodimers were examined as described in Scheme 2, wherein different substituents were placed on the two methyl groups. The X substituents are thought to be electron-releasing, while various withdrawing agents Y were placed on the other methyl.

As may be seen in Table 7, the R(C···C) distances are all close to one another, around 3.4 Å, and the geometries adhere closely to a linear XC···CY alignment. The first six rows of Table 7 indicate there is very little variation in the interaction energy whether X is NH_2 or NCH_3, nor does this measure of bond

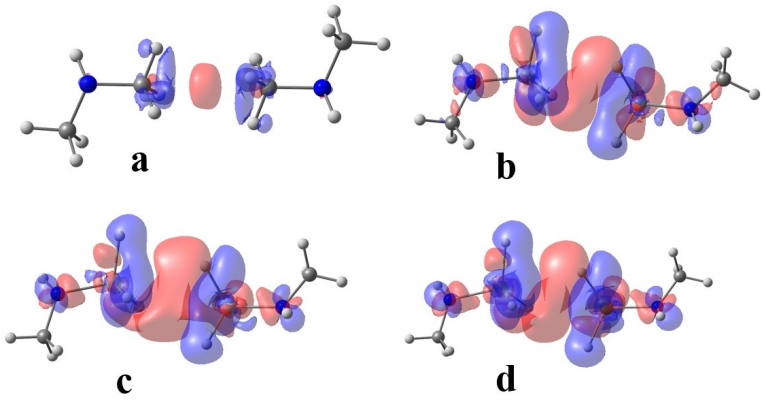

Figure 6. Density gains (red) and losses (blue) that accompany formation of dimer from separated monomers in a) $(CH_3NHCH_3)_2$, b) $(CH_3NHSiH_3)_2$, c) $(CH_3NHGeH_3)_2$, and d) $(CH_3NHSnH_3)_2$. Surface shown corresponds to 0.0001 au.

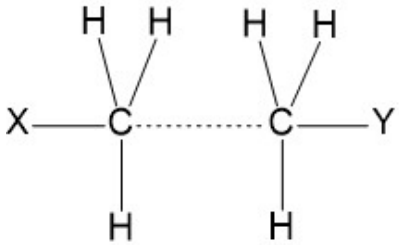

X= NH_2, NCH_3, $B(CH_3)_2$, $Al(CH_3)_2$, $Ga(CH_3)_2$;
Y= CF_3, NO_2, CN, Cl, Br, I.

Scheme 2. Heterodimers studied.

strength depend upon the nature of the electron-withdrawing group Y, whether CF_3, NO_2, or CN. The last two columns of Table 7 document the σ-hole depths on the methyl C atoms as defined as the maximum of the MEP on a 0.001 au isodensity surface. V_X is rather shallow for the electron-donating species, less than 4 kcal/mol. V_Y on the other species is deeper, particularly for CH_3NO_2 where it reaches up to 29 kcal/mol. Nonetheless, E_{int} is fairly steady, varying only slightly with V_Y.

The situation changes a bit for the more electron-releasing $TrMe_2$ species in the next sections of Table 7 where Tr refers to the triel atoms B, Al, and Ga. Their donation reverses the sign of the MEP of the methyl C, leading to the negative quantities for V_X which are in fact minima on the surface. The juxtaposition of these negative potentials with the positive V_Y of the partner species lead to more significant growth in the interaction energy. In comparison to the −0.5 kcal/mol values in the upper portion of the table, E_{int} rises to as high as −1.3 kcal/mol. While still a fairly weak interaction, this quantity has nearly tripled in magnitude. Indeed, even though the total electrostatic term may contribute only a limited amount to the total interaction, there is a very close connection between E_{int} and the product of the two potentials, $Vx*V_Y$, as is evident in Figure 7. The correlation coefficient R^2 between these two quantities is 0.996.

Earlier calculations[9a,12b] support the idea that an asymmetry between X and Y can strengthen a methyl···methyl interaction. Keshtkar et al[12b] obtained interaction energies of the same order as in Table 7 for Me_2M species X where M=Si, Sn, and Al, and Y taken from Me, NMe_2, OMe, and Br. When a F atom was added to one methyl group, and a strongly electron-releasing Li to the other,[9a] an interaction energy of 2.9 kcal/mol was calculated, even larger than the quantities listed in Table 7. This enhanced interaction was due in large part to the high potency of Li as electron releasing agent.

Conclusions

Methyl groups can form attractive interactions with one another, albeit weak ones in the neighborhood of 1 kcal/mol. The interaction energies can be ramped up to 2 or 3 kcal/mol by exchanging the C atom for any of the larger tetrels. The binding is strongest if the tetrel atom is attached to the smallest and most electronegative pnicogen atom N. A certain degree of enhancement can be achieved in asymmetric systems wherein one methyl group is bonded to an electron-withdrawing substituent, and the other to an electron donor. The geometries involving the larger tetrel atoms are not fully linear, but offset a bit which leads to structures where the H atoms interact directly with one another, rather than a T···T interaction. AIM, NCI, and NBO analyses are at odds as to whether a true tetrel bond is present in these offset configurations. The latter tools must be employed cautiously as they can suggest the presence of a strong attraction when the potential is in fact repulsive.

Acknowledgements

The authors gratefully acknowledge Polish high-performance computing infrastructure PLGrid (HPC Centers: ACK Cyfronet AGH) for providing computer facilities and support within computational grant no. PLG/2023/016853, Wrocław Center for

Table 7. Selected structural parameters (distance in Å, angles in degs), interaction energy and molecular electrostatic potential extrema (kcal/mol) at C atom of methyl group of optimized monomer.

X	Y	R(C···C)	θ(X–C···C)	θ(Y–C···C)	E_{int}	V_X[a]	V_Y
NH_2	CF_3	3.394	175.0	178.3	−0.46	3.0	17.0
NH_2	NO_2	3.331	175.5	177.0	−0.49	3.0	29.3
NH_2	CN	3.383	175.8	178.5	−0.49	3.0	23.6
$N(CH_3)_2$	CF_3	3.390	179.3	179.3	−0.47	3.7	17.0
$N(CH_3)_2$	NO_2	3.333	173.2	169.8	−0.53	3.7	29.3
$N(CH_3)_2$	CN	3.375	179.3	179.4	−0.50	3.7	23.6
$B(CH_3)_2$	Cl	3.388	179.7	177.0	−0.74	−6.3	17.3
$B(CH_3)_2$	Br	3.403	178.1	176.8	−0.73	−6.3	16.5
$B(CH_3)_2$	I	3.428	178.3	178.4	−0.67	−6.3	13.6
$B(CH_3)_2$	NO_2	3.364	178.1	178.8	−0.94	−6.3	29.3
$Al(CH_3)_2$	Cl	3.403	179.0	177.8	−0.94	−11.1	17.3
$Al(CH_3)_2$	Br	3.420	178.8	178.4	−0.92	−11.1	16.5
$Al(CH_3)_2$	I	3.440	178.6	176.2	−0.84	−11.1	13.6
$Al(CH_3)_2$	NO_2	3.374	178.1	177.9	−1.27	−11.1	29.3
$Ga(CH_3)_2$	Cl	3.390	179.6	178.2	−0.93	−10.5	17.3
$Ga(CH_3)_2$	Br	3.409	178.3	179.0	−0.92	−10.5	16.5
$Ga(CH_3)_2$	I	3.422	178.3	178.2	−0.84	−10.5	13.6
$Ga(CH_3)_2$	NO_2	3.362	179.6	177.3	−1.26	−10.5	29.3

[a] V_{max} and V_{min} signified by positive and negative values, respectively.

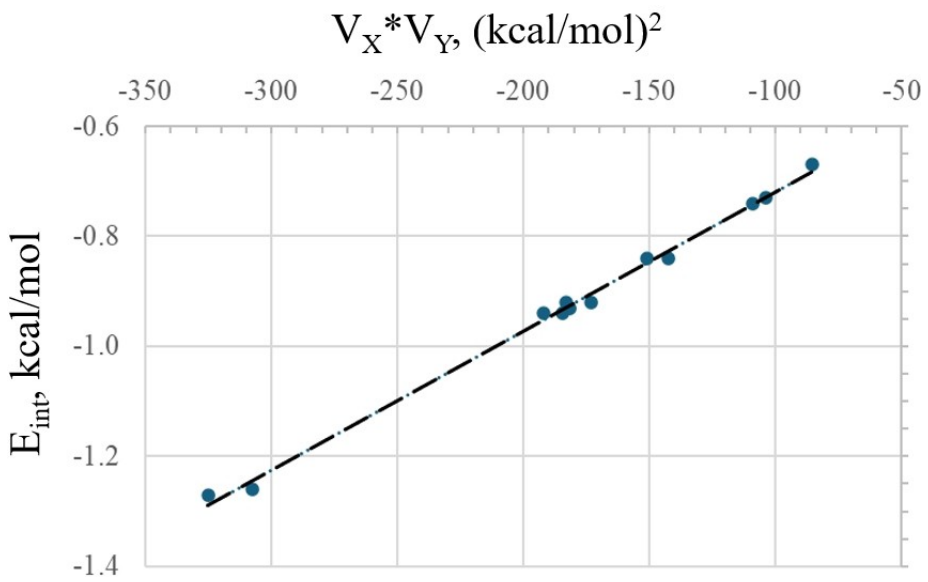

Figure 7. Relationship between interaction energy and product of MEP extrema on monomers.

Networking and Supercomputing (WCSS). This material is also based upon work supported by the U.S. National Science Foundation under Grant No. 1954310 to SS. This work was financed in part by a statutory activity subsidy from the Polish Ministry of Science and Higher Education for the Faculty of Chemistry of Wroclaw University of Science and Technology.

Conflict of Interests

The authors declare no conflict of interest.

Data Availability Statement

The data that support the findings of this study are available in the supplementary material of this article.

Keywords: Tetrel bond · Molecular electrostatic potential · Energy decomposition

[1] a) S. Scheiner, *Hydrogen Bonding: A Theoretical Perspective*, Oxford University Press, New York **1997**; b) G. A. Jeffrey, G. A. Jeffrey, *An Introduction to Hydrogen Bonding, Vol. 12*, Oxford university press, New York **1997**.
[2] a) P. Politzer, J. S. Murray, T. Clark, *Phys. Chem. Chem. Phys.* **2021**, *23*, 16458–16468; b) P. Politzer, J. S. Murray, *Theor. Chem. Acc.* **2021**, *140*, 7; c) P. Politzer, J. S. Murray, *Chemphyschem* **2020**, *21*, 579–588; d) J. S. Murray, P. Lane, P. Politzer, *J. Mol. Model.* **2009**, *15*, 723–729; e) J. S. Murray, P. Lane, T. Clark, P. Politzer, *J. Mol. Model.* **2007**, *13*, 1033–1038; f) T. Clark, M. Hennemann, J. S. Murray, P. Politzer, *J. Mol. Model.* **2007**, *13*, 291–296.
[3] A. Bauza, T. J. Mooibroek, A. Frontera, *ChemPhysChem* **2015**, *16*, 2496–2517.
[4] a) S. Scheiner, *Phys. Chem. Chem. Phys.* **2021**, *23*, 5702–5717; b) A. Daolio, P. Scilabra, G. Terraneo, G. Resnati, *Coord. Chem. Rev.* **2020**, *413*, 213265; c) A. Bauza, T. J. Mooibroek, A. Frontera, *Chem. Rec.* **2016**, *16*, 473–487.
[5] a) M. D. Piña, A. K. Sahu, A. Frontera, H. S. Biswal, A. Bauzá, *Phys. Chem. Chem. Phys.* **2023**, *25*, 12409–12419; b) M. S. Taylor, *Coord. Chem. Rev.* **2020**, *413*, 213270; c) S. Scheiner, *Molecules* **2018**, *23*, 1147.
[6] a) D. Majumdar, A. Frontera, R. M. Gomila, S. Das, K. Bankura, *RSC Adv.* **2022**, *12*, 6352–6363; b) A. Daolio, E. K. Wieduwilt, A. Pizzi, A. Genoni, G. Resnati, G. Terraneo, *Phys. Chem. Chem. Phys.* **2022**, *24*, 24892–24901; c) G. Mahmoudi, M. Abedi, S. E. Lawrence, E. Zangrando, M. G. Babashkina, A. Klein, A. Frontera, D. A. Safin, *Molecules* **2020**, *25*, 4056.
[7] a) J. J. Roeleveld, S. J. Lekanne Deprez, A. Verhoofstad, A. Frontera, J. I. van der Vlugt, T. J. Mooibroek, *Chemistry* **2020**, *26*, 10126–10132; b) F. A. Afkhami, G. Mahmoudi, F. R. Qu, A. Gupta, M. Kose, E. Zangrando, F. I. Zubkov, I. Alkorta, D. A. Safin, *Crystengcomm* **2020**, *22*, 2389–2396.
[8] S. J. Grabowski, *Phys. Chem. Chem. Phys.* **2014**, *16*, 1824–1834.
[9] a) S. Scheiner, *Phys. Chem. Chem. Phys.* **2020**, *22*, 16606–16614; b) W. Zierkiewicz, M. Michalczyk, G. Mahmoudi, I. Garcia-Santos, A. Castineiras, E. Zangrando, S. Scheiner, *Chemphyschem* **2022**, *23*, e202200306; c) A. Grabarz, M. Michalczyk, W. Zierkiewicz, S. Scheiner, *Chemphyschem* **2020**, *21*, 1934–1944; d) S. Scheiner, *Polyhedron* **2021**, *193*, 114905
[10] a) A. Razin, H. Cedar, *Microbiol. Rev.* **1991**, *55*, 451–458; b) W. Aufsatz, M. F. Mette, J. Van Der Winden, A. J. M. Matzke, M. Matzke, *Proc. Natl. Acad. Sci. U. S. A.* **2002**, *99*, 16499–16506.
[11] L. C. Sowers, B. R. Shaw, W. D. Sedwick, *Biochem. Biophys. Res. Commun.* **1987**, *148*, 790–794.
[12] a) H.-Y. Zhuo, L.-X. Jiang, Q.-Z. Li, W.-Z. Li, J.-B. Cheng, *Chem. Phys. Lett.* **2014**, *608*, 90–94; b) N. Keshtkar, O. Loveday, V. Polo, J. Echeverría, *Cryst. Growth Des.* **2023**, *23*, 5112–5116.
[13] a) A. Bauza, T. J. Mooibroek, A. Frontera, *Angew. Chem. Int. Ed.* **2013**, *52*, 12317–12321; b) A. Frontera, *C-J Carbon Res.* **2020**, *6*; c) Alvarez, *Inorg. Chem.* **2022**, *61*, 9082–9095; d) N. Mahapatra, S. Chandra, N. Ramanathan, K. Sundararajan, *Chemistryselect* **2023**, *8*, e202302817; e) P. Ramasami, T. A. Ford, *Comput. Theor. Chem.* **2023**, *1220*, 114021; f) R. C. Trievel, S. Scheiner, *Molecules* **2018**, *23*, 2965; g) T. J. Mooibroek, *Molecules* **2019**, *24*, 3370.
[14] a) O. Loveday, J. Echeverria, *Nat. Commun.* **2021**, *12*, 5030; b) J. Echeverria, *Crystengcomm* **2017**, *19*, 6289–6296.
[15] O. Loveday, J. Echeverría, *Cryst. Growth Des.* **2021**, *21*, 5961–5966.
[16] J. Damián, C. Rentero, J. Echeverría, M. E. G. Mosquera, *Faraday Discuss.* **2023**, *244*, 294–305.
[17] F. Teixidor, G. Barberà, A. Vaca, R. Kivekäs, R. Sillanpää, J. Oliva, C. Viñas, *J. Am. Chem. Soc.* **2005**, *127*, 10158–10159.
[18] a) S. Scheiner, *Crystengcomm* **2023**, *25*, 5060–5071; b) S. Scheiner, *J. Comput. Chem.* **2022**, *43*, 1814–1824.
[19] a) F. Weigend, *Phys. Chem. Chem. Phys.* **2006**, *8*, 1057–1065; b) F. Weigend, R. Ahlrichs, *Phys. Chem. Chem. Phys.* **2005**, *7*, 3297–3305; c) Y. Zhao, D. G. Truhlar, *Acc. Chem. Res.* **2008**, *41*, 157–167; d) Y. Zhao, D. G. Truhlar, *Theor. Chem. Acc.* **2008**, *120*, 215–241.
[20] M. J. Frisch, G. W. Trucks, H. B. Schlegel, G. E. Scuseria, M. A. Robb, J. R. Cheeseman, G. Scalmani, V. Barone, G. A. Petersson, H. Nakatsuji, X. Li, M. Caricato, A. V. Marenich, J. Bloino, B. G. Janesko, R. Gomperts, B. Mennucci, H. P. Hratchian, J. V. Ortiz, A. F. Izmaylov, J. L. Sonnenberg, Williams, F. Ding, F. Lipparini, F. Egidi, J. Goings, B. Peng, A. Petrone, T. Henderson, D. Ranasinghe, V. G. Zakrzewski, J. Gao, N. Rega, G. Zheng, W. Liang, M. Hada, M. Ehara, K. Toyota, R. Fukuda, J. Hasegawa, M. Ishida, T. Nakajima, Y. Honda, O. Kitao, H. Nakai, T. Vreven, K. Throssell, J. A. Montgomery Jr., J. E. Peralta, F. Ogliaro, M. J. Bearpark, J. J. Heyd, E. N. Brothers, K. N. Kudin, V. N. Staroverov, T. A. Keith, R. Kobayashi, J. Normand, K. Raghavachari, A. P. Rendell, J. C. Burant, S. S. Iyengar, J. Tomasi, M. Cossi, J. M. Millam, M. Klene, C. Adamo, R. Cammi, J. W. Ochterski, R. L. Martin, K. Morokuma, O. Farkas, J. B. Foresman, D. J. Fox, Wallingford, CT, Revision C.01 **2016**.
[21] C. R. Groom, I. J. Bruno, M. P. Lightfoot, S. C. Ward, *Acta Crystallogr. B* **2016**, *72*, 171–179.
[22] S. F. Boys, F. Bernardi, *Mol. Phys.* **1970**, *19*, 553–566.
[23] a) T. Lu, F. Chen, *J. Mol. Graphics Model.* **2012**, *38*, 314–323; b) T. Lu, F. Chen, *J. Comput. Chem.* **2012**, *33*, 580–592.
[24] W. Humphrey, A. Dalke, K. Schulten, *J. Mol. Graphics Model.* **1996**, *14*, 33–38.
[25] A. T. Keith, TK Gristmill Software, Overland Park KS, USA, version 19.10.12, Professional **2014**.
[26] a) R. Bader, *Atoms in Molecules. A Quantum Theory*, Clarendon Press, Oxford **1990**; b) R. F. W. Bader, *J. Phys. Chem. A* **1998**, *102*, 7314–7323.
[27] F. Weinhold, C. R. Landis, E. D. Glendening, *Int. Rev. Phys. Chem.* **2016**, *35*, 399–440.
[28] a) P. R. Horn, Y. Mao, M. Head-Gordon, *Phys. Chem. Chem. Phys.* **2016**, *18*, 23067–23079; b) P. R. Horn, Y. Mao, M. Head-Gordon, *J. Chem. Phys.* **2016**, *144*, 114107.
[29] M. Podsiadło, A. Olejniczak, A. Katrusiak, *Cryst. Growth Des.* **2017**, *17*, 2218–2222.
[30] S. M. Godfrey, C. A. McAuliffe, R. G. Pritchard, S. Sarwar, *J. Chem. Soc. Dalton Trans.* **1997**, *6*, 1031–1036.

Manuscript received: April 30, 2024
Revised manuscript received: September 25, 2024
Accepted manuscript online: October 1, 2024
Version of record online: November 8, 2024